

Assessment of long-range-corrected exchange-correlation kernels for solids: Accurate exciton binding energies via an empirically scaled bootstrap kernel

Young-Moo Byun and Carsten A. Ullrich*

Department of Physics and Astronomy, University of Missouri, Columbia, Missouri 65211, USA

(Received 5 March 2017; revised manuscript received 26 April 2017; published 22 May 2017)

In time-dependent density-functional theory, a family of exchange-correlation kernels, known as long-range-corrected (LRC) kernels, have shown promise in the calculation of excitonic effects in solids. We perform a systematic assessment of existing static LRC kernels (empirical LRC, Bootstrap, and jellium-with-a-gap model) for a range of semiconductors and insulators, focusing on optical spectra and exciton binding energies. We find that no LRC kernel is capable of simultaneously producing good optical spectra and quantitatively accurate exciton binding energies for both semiconductors and insulators. We propose a simple and universal, empirically scaled Bootstrap kernel that yields accurate exciton binding energies for all materials under consideration, with low computational cost.

DOI: [10.1103/PhysRevB.95.205136](https://doi.org/10.1103/PhysRevB.95.205136)

I. INTRODUCTION

The optical properties of insulators and semiconductors in the energy range close to the gap are strongly influenced by excitons. The accurate and efficient calculation of excitonic properties is an important task of computational materials science, since it is a key requirement in the design of novel photovoltaic materials of desired properties. For example, low exciton binding energies in perovskite solar cells promote the electron-hole separation and thereby enhance power conversion efficiencies [1].

Many-body perturbation theory is a standard theoretical method for excitonic effects in solids: accurate exciton binding energies E_b and optical absorption spectra of semiconductors and insulators are obtained by solving the Bethe-Salpeter equation (BSE) [2–4]. However, the BSE is computationally too expensive to be applied to large systems. Time-dependent density-functional theory (TDDFT) [5–7] provides alternatives to the BSE, which are computationally much cheaper.

The main challenge for TDDFT lies in finding approximations to the exchange-correlation (xc) kernel f_{xc} , which yield accurate excitonic properties. The random-phase approximation (RPA) ($f_{xc} = 0$), the local-density approximation (LDA), and generalized gradient approximations (GGAs) fail to capture excitonic effects in solids due to their inadequate long-range behavior. The so-called “nanoquanta kernel” [8–11], constructed by reverse-engineering the BSE, yields very good optical spectra of solids and thus provides an important proof of principle; however, it is computationally as expensive as the BSE.

Hybrid xc functionals (mixtures of semilocal xc functionals with a fraction of nonlocal Fock exchange) are very widely used in TDDFT. The B3LYP hybrid functional [12] gives reasonably good optical spectra for systems whose gap is not too large [13,14]. For organic molecular crystals, the so-called optimally tuned range-separated hybrids produce excellent results [15]. A scaled exact exchange approach was recently shown to yield good excitonic binding energies for a wide variety of materials [16]. However, the nonlocal exchange

contribution adds to the computational cost of the hybrid methods; it is therefore desirable to work with purely local xc functionals.

A simple nonlocal model kernel, which is known as the long-range-corrected (LRC) kernel [8,17,18],

$$f_{xc}^{\text{LRC}} = -\frac{\alpha}{\mathbf{q}^2}, \quad (1)$$

where \mathbf{q} is the momentum transfer in the first Brillouin zone (BZ), can account for bound excitons in solids, but it requires a material-dependent parameter α , a positive scalar. A number of nonempirical xc kernels proposed in the literature, namely the Bootstrap [19], RPA-Bootstrap [20], and jellium-with-gap-model (JGM) kernels [21], report that the long-range part in them gives the most important contribution to their results for optical spectra in solids. Thus, in spite of their diversity, these kernels can essentially be viewed as somewhat more sophisticated LRC kernels, as explicitly stated in Refs. [19] and [21]. Hence, in this paper we refer to all of the above xc kernels [17–21] as the family of LRC-type kernels. These kernels have been applied to simple bulk semiconductors and insulators, with some degree of success. However, there also were reports of conflicting results, giving rise to some recent controversies in the literature [22,23].

Testing the performance of the various LRC-type kernels is a complex task that depends on many choices. For instance, the xc kernel, which is formally a matrix in reciprocal space, can be implemented as head-only, diagonal, or a full matrix. Local-field effects can be fully or partially included or completely ignored. The calculated optical spectra depend on the input band structure (LDA with or without scissors correction, GGA, LDA+U, hybrids, or GW) and on the method (such as all-electron versus pseudopotential-based). And, last but not least, the selection of the materials is important. Given the large number of choices that have to be made, an unbiased assessment and a comparison between different LRC methods is challenging, and conflicting results can arise.

In this paper, we will perform a systematic assessment of the various existing *static* LRC-type kernels (i.e., we do not assess *dynamical* LRC-type kernels such as those proposed in Refs. [24], [25]), for a variety of materials ranging from small-gap semiconductors to large-gap insulators, comparing

*ullrichc@missouri.edu

calculated optical spectra and exciton binding energies to experimental data. The main finding is that the existing LRC-type kernels, while often producing good-looking optical spectra for semiconductors, all fail to yield consistently good exciton binding energies. We propose an empirical scaling approach, to be used in conjunction with the RPA-Bootstrap method, which gives accurate E_b for all materials under study, but the resulting optical spectra may have unsatisfactory distributions of oscillator strength.

This paper is organized as follows. In Sec. II, we give an overview of the formal framework of linear-response TDDFT, comparing two approaches to describe optical properties of solids: the Dyson-equation approach and the Casida equation. We then review the existing static LRC-type xc kernels and the different choices for their implementation. We also discuss some computational details. Section III then presents our results. We demonstrate the sensitivity of the optical spectra to the choice of the α -parameter and then propose a scaled RPA-Bootstrap kernel which gives accurate exciton binding energies. Section IV contains our conclusions.

II. BACKGROUND AND METHODOLOGY

A. Linear-response TDDFT for solids: Dyson equation versus Casida equation approach

There are several ways to calculate optical absorption spectra of periodic systems using linear-response TDDFT [6]. The most common approach is based on the interacting density-density response function $\chi_{\mathbf{G}\mathbf{G}'}(\mathbf{q}, \omega)$, where \mathbf{G} and \mathbf{G}' are reciprocal lattice vectors, and ω is the frequency. The response function is obtained from the following Dyson-type equation:

$$\chi_{\mathbf{G}\mathbf{G}'}(\mathbf{q}, \omega) = \chi_{\mathbf{G}\mathbf{G}'}^{(0)}(\mathbf{q}, \omega) + \sum_{\mathbf{G}_1 \mathbf{G}_2} \chi_{\mathbf{G}\mathbf{G}_1}^{(0)}(\mathbf{q}, \omega) \times [V_{\mathbf{G}_1}(\mathbf{q})\delta_{\mathbf{G}_1 \mathbf{G}_2} + f_{xc, \mathbf{G}_1 \mathbf{G}_2}(\mathbf{q})]\chi_{\mathbf{G}_2 \mathbf{G}'}(\mathbf{q}, \omega), \quad (2)$$

where $\chi^{(0)}$ is the noninteracting response function and $V_{\mathbf{G}}(\mathbf{q}) = 4\pi/|\mathbf{q} + \mathbf{G}|^2$ is the Coulomb interaction. It is convenient to write $V = V_0 + \bar{V}$, where V_0 is the long-range ($\mathbf{G} = 0$) part of the Coulomb interaction, and \bar{V} is the Coulomb interaction without the long-range part. $f_{xc, \mathbf{G}\mathbf{G}'}$ is the xc kernel in the adiabatic approximation, i.e., independent of ω . $\chi^{(0)}$ is explicitly given by [26]

$$\begin{aligned} \chi_{\mathbf{G}\mathbf{G}'}^{(0)}(\mathbf{q}, \omega) &= \frac{2}{\mathcal{V}} \sum_{nm\mathbf{k}} (f_{m\mathbf{k}+\mathbf{q}} - f_{n\mathbf{k}}) \\ &\times \frac{\langle m\mathbf{k} + \mathbf{q} | e^{i(\mathbf{k}+\mathbf{G})\cdot\mathbf{r}} | n\mathbf{k} \rangle \langle n\mathbf{k} | e^{-i(\mathbf{k}+\mathbf{G}')\cdot\mathbf{r}'} | m\mathbf{k} + \mathbf{q} \rangle}{E_{m\mathbf{k}+\mathbf{q}} - E_{n\mathbf{k}} - (\omega + i\eta)}, \end{aligned} \quad (3)$$

where \mathbf{k} lies within the first BZ, n and m are band indices, $E_{n\mathbf{k}}$ and $E_{m\mathbf{k}+\mathbf{q}}$ are the associated Kohn-Sham single-particle energies, $f = 1(0)$ for occupied (unoccupied) states, the factor of 2 accounts for the spin (we here only consider non-spin-polarized systems), \mathcal{V} is the crystal volume, and η is an infinitesimal. In the optical limit ($\mathbf{q} \rightarrow 0$), the head

($\mathbf{G} = \mathbf{G}' = 0$) of $\chi^{(0)}$ at $\omega = 0$ becomes [27]

$$\chi_{00}^{(0)}(\mathbf{q} \rightarrow 0, 0) = -\frac{4\mathbf{q}^2}{\mathcal{V}} \sum_{vck} \frac{|\langle c\mathbf{k} | \hat{p} + i[V_{\text{NL}}, \hat{r}] | v\mathbf{k} \rangle|^2}{(E_{c\mathbf{k}} - E_{v\mathbf{k}})^3}, \quad (4)$$

where v and c are valence and conduction band indices, respectively, \hat{p} is the momentum operator, \hat{r} is the position operator, and V_{NL} is the nonlocal part of the pseudopotential. The \mathbf{q}^2 -dependence will be important for the construction of the Bootstrap kernels; see below. It is also important that $\chi_{00}^{(0)}(\mathbf{q} \rightarrow 0, 0)$ is always negative.

The optical spectrum is obtained from the imaginary part of the macroscopic dielectric function ϵ_M :

$$\epsilon_M(\omega) = \lim_{\mathbf{q} \rightarrow 0} \frac{1}{\epsilon_{00}^{-1}(\mathbf{q}, \omega)} \quad (5)$$

$$= \lim_{\mathbf{q} \rightarrow 0} \frac{1}{1 + V_0(\mathbf{q})\chi_{00}(\mathbf{q}, \omega)}, \quad (6)$$

where ϵ^{-1} is the inverse dielectric function [3]. We shall refer to this method as the Dyson approach; it has a moderate computational cost and is therefore the method of choice for calculating optical spectra. However, the drawback of the Dyson-equation approach is that fine details of the spectra, in particular the binding energies of weakly bound excitons, cannot be obtained, because the spectral broadening, which is applied after calculating $\epsilon_M(\omega)$ at each ω point to produce a continuous and smooth optical spectrum, washes out any subtle features of the order of a few meV (see also Sec. II C).

As an alternative that is strictly equivalent to the Dyson equation, optical spectra and exciton binding energies can be obtained from the Casida equation [28]:

$$\begin{pmatrix} \mathbf{A} & \mathbf{B} \\ \mathbf{B}^* & \mathbf{A}^* \end{pmatrix} \begin{pmatrix} X_n \\ Y_n \end{pmatrix} = \omega_n \begin{pmatrix} -1 & \mathbf{0} \\ \mathbf{0} & \mathbf{1} \end{pmatrix} \begin{pmatrix} X_n \\ Y_n \end{pmatrix}, \quad (7)$$

where \mathbf{A} and \mathbf{B} are excitation and de-excitation matrices, respectively, X_n and Y_n are n th eigenvectors, and ω_n is the n th excitation energy. The matrix elements of \mathbf{A} and \mathbf{B} are given by

$$A_{vck, v'c'k'} = (E_{c\mathbf{k}} - E_{v\mathbf{k}})\delta_{vv'}\delta_{cc'}\delta_{\mathbf{k}\mathbf{k}'} + F_{vck, v'c'k'}^{\text{Hxc}}, \quad (8)$$

$$B_{vck, v'c'k'} = F_{vck, v'c'k'}^{\text{Hxc}}, \quad (9)$$

where $F^{\text{Hxc}} = F^{\text{H}} + F^{\text{xc}}$ is the Hartree-exchange-correlation (Hxc) matrix [5]. The matrix dimension of the Casida Eq. (7) is proportional to the number of \mathbf{k} -points, which makes it computationally quite demanding (see Sec. II C for more details).

In the optical limit, F^{H} and F^{xc} are given by

$$F_{vck, v'c'k'}^{\text{H}} = \frac{2}{\mathcal{V}} \sum_{\mathbf{G} \neq 0} \frac{4\pi}{|\mathbf{G}|^2} \langle c\mathbf{k} | e^{i\mathbf{G}\cdot\mathbf{r}} | v\mathbf{k} \rangle \langle v'\mathbf{k}' | e^{-i\mathbf{G}\cdot\mathbf{r}'} | c'\mathbf{k}' \rangle, \quad (10)$$

$$\begin{aligned} F_{vck, v'c'k'}^{\text{xc}} &= \frac{2}{\mathcal{V}} \lim_{\mathbf{q} \rightarrow 0} \sum_{\mathbf{G}\mathbf{G}'} f_{xc, \mathbf{G}\mathbf{G}'}(\mathbf{q}) \langle c\mathbf{k} | e^{i(\mathbf{q}+\mathbf{G})\cdot\mathbf{r}} | v\mathbf{k} \rangle \\ &\times \langle v'\mathbf{k}' | e^{-i(\mathbf{q}+\mathbf{G}')\cdot\mathbf{r}'} | c'\mathbf{k}' \rangle. \end{aligned} \quad (11)$$

For the elements of F^{xc} in Eq. (11) to remain finite (i.e., neither vanishing nor diverging) in the $\mathbf{q} \rightarrow 0$ limit, the head ($\mathbf{G} = \mathbf{G}' = 0$) of f_{xc} should be proportional to \mathbf{q}^{-2} , the wings

($\mathbf{G} = 0, \mathbf{G}' \neq 0$ or vice versa) should be proportional to \mathbf{q}^{-1} , and the body ($\mathbf{G}, \mathbf{G}' \neq 0$) should be independent of \mathbf{q} (see Refs. [29] and [30] for more details). In other words, the most general form is

$$\lim_{\mathbf{q} \rightarrow 0} f_{xc, \mathbf{G}\mathbf{G}'}(\mathbf{q}) = \begin{pmatrix} \frac{\kappa_{00}}{\mathbf{q}^2} & \frac{\kappa_{01}}{\mathbf{q}} & \frac{\kappa_{02}}{\mathbf{q}} & \dots \\ \frac{\kappa_{10}}{\mathbf{q}} & \kappa_{11} & \kappa_{12} & \dots \\ \frac{\kappa_{20}}{\mathbf{q}} & \kappa_{21} & \kappa_{22} & \dots \\ \vdots & \vdots & \vdots & \ddots \end{pmatrix}, \quad (12)$$

where the $\kappa_{\mathbf{G}\mathbf{G}'}$ are constants (in general, they are functionals of the density). We will discuss various approximations of the xc kernel in the following subsection.

The excitation energy spectrum ω_n of the Casida equation, Eq. (7), for periodic solids with a gap has discrete levels, which correspond to bound excitons, and a continuous part, which corresponds to the unbound particle-hole excitations. For the adiabatic xc kernels considered here, only one excitonic level is found, which can be identified as the lowest bound exciton (to obtain an excitonic Rydberg series with a scalar xc kernel requires the kernel to be frequency-dependent) [31,32]. We calculate the exciton binding energy as that energy which separates this discrete level from the onset of the continuum. Since no artificial spectral broadening is involved, exciton binding energies can be calculated in principle with arbitrary precision. However, the Casida-equation approach is computationally expensive because it requires building and diagonalizing a large matrix.

Note that by using a very small broadening width and a very fine frequency grid, one may be able to obtain E_b of semiconductors from the Dyson-equation optical spectrum, but the broadening width and the frequency grid spacing always cause an error that may be greater than E_b of interest. (The truncation of Dyson-equation and Casida-equation matrices, which are in principle infinite dimensional, also results in error, but this error is more closely related to the convergence behavior than to the difference between Dyson and Casida approaches; see Sec. II C.) Note also that Ref. [20] proposed a method to “read” E_b from the real part of $\epsilon_M^{\text{RPA}}(\omega)$, but this approach works only for head-only kernels and only for wide-gap insulators (i.e., one cannot obtain small E_b on the order of a few meV), and it has a moderate precision (~ 0.1 eV). By contrast, the Casida equation works for all forms of the xc kernel and for all materials, and it has a high precision (~ 0.01 meV).

A widely used approach to simplify the Casida equation is the so-called Tamm-Dancoff approximation (TDA), which decouples excitations and de-excitations by setting \mathbf{B} to zero in Eq. (7). However, we have found [33] that the TDA underestimates LRC E_b of insulators significantly (i.e., by more than 100%) (e.g., TDA and full Casida equations using the RPA-Bootstrap kernel without the scissors shift yield $E_b = 666$ and 2400 meV, respectively, for solid Ne), so we will only use the full Casida equation in this work.

The local-field effect (LFE) is determined by the number of \mathbf{G} vectors included and has different forms in the Dyson and Casida equations. In the Dyson approach, the LFE means including not only the head, but also the wings and body of the matrix in \mathbf{G}, \mathbf{G}' , which leads to $\epsilon_{00} \neq 1/\epsilon_{00}^{-1}$. The Dyson equation is used to calculate optical spectra and Bootstrap-

type kernel parameters (more about this later). In the Dyson equation for optical spectra, the LFE is not a matter of choice and should be included. However, in the Dyson equation for Bootstrap-type kernel parameters, the LFE is a matter of choice because of the freedom of defining Bootstrap-type kernels. In this work, we will include the LFE when calculating Bootstrap-type kernel parameters, following the convention adopted in the literature [19].

In the Casida equation, the LFE means including not only the head, but also other terms in the summation of F^{Hxc} matrix elements in Eqs. (11) and (16). Mathematically, the LFE in the Dyson equation is exactly transformed into the summation in the Casida equation. Therefore, if the LFE is included in the Dyson equation, it should be included in the Casida equation, too.

B. LRC-type xc kernels

In reciprocal space, the xc kernels $f_{xc, \mathbf{G}\mathbf{G}'}(\mathbf{q})$ are matrices in \mathbf{G} and \mathbf{G}' ; see Eq. (12). In the following, we list the xc kernels we have tested, paying particular attention to distinguish between head-only, diagonal, or full matrix forms. In all expressions, the optical limit ($\mathbf{q} \rightarrow 0$) is understood.

1. Empirical LRC kernel

The empirical LRC kernel was originally designed as a kernel for optical spectra of semiconductors [8]. The diagonal and the head-only versions of the empirical LRC kernel are defined, respectively, as

$$f_{xc}^{\text{LRC(d)}} = -\frac{\alpha}{4\pi} V = \begin{pmatrix} -\frac{\alpha}{\mathbf{q}^2} & 0 & 0 & \dots \\ 0 & -\frac{\alpha}{G_1^2} & 0 & \dots \\ 0 & 0 & -\frac{\alpha}{G_2^2} & \dots \\ \vdots & \vdots & \vdots & \ddots \end{pmatrix} \quad (13)$$

and

$$f_{xc}^{\text{LRC(h)}} = -\frac{\alpha}{4\pi} V_0 = \begin{pmatrix} -\frac{\alpha}{\mathbf{q}^2} & 0 & 0 & \dots \\ 0 & 0 & 0 & \dots \\ 0 & 0 & 0 & \dots \\ \vdots & \vdots & \vdots & \ddots \end{pmatrix}. \quad (14)$$

Here, α is an empirical parameter, given by [17]

$$\alpha_{\text{LRC}} = \frac{C_1}{\epsilon_\infty} - C_2, \quad (15)$$

where $C_1 = 4.615$, $C_2 = 0.213$, and ϵ_∞ is the high-frequency dielectric constant. Note that here we use $\epsilon_{\text{RPA}}^{-1}$ instead of the experimental $1/\epsilon_\infty$, where $\epsilon_{\text{RPA}}^{-1}$ is greater than $1/\epsilon_\infty$ by $\sim 10\%$. Also note that the empirical LRC kernel used calculated lattice parameters, while we take experimental ones. Due to these differences, empirical parameters C_1 and C_2 should be refitted to our choices, but it turns out that such differences make little effect on LRC results for semiconductors (see below).

In general, when a head-only or diagonal LRC kernel is used, F^{Hxc} simplifies to

$$F_{v\mathbf{k},v'\mathbf{k}'}^{\text{Hxc}} = \frac{2}{\mathcal{V}} \left(\sum_{\mathbf{G} \neq 0} \frac{4\pi - \bar{\alpha}}{|\mathbf{G}|^2} \langle \mathbf{k} | e^{i\mathbf{G}\cdot\mathbf{r}} | v\mathbf{k} \rangle \langle v'\mathbf{k}' | e^{-i\mathbf{G}\cdot\mathbf{r}} | c'\mathbf{k}' \rangle - \alpha_0 \frac{\langle \mathbf{k} | \hat{p} + i[V_{\text{NL}}, \hat{r}] | v\mathbf{k} \rangle \langle c'\mathbf{k}' | \hat{p} + i[V_{\text{NL}}, \hat{r}] | v'\mathbf{k}' \rangle^*}{E_{c\mathbf{k}} - E_{v\mathbf{k}}} \right), \quad (16)$$

where $\alpha = \alpha_0$ and $\bar{\alpha} = 0$ for the head-only kernel $f_{\text{xc}}^{\text{LRC(h)}}$, and $\alpha = \alpha_0 = \bar{\alpha}$ for the diagonal kernel $f_{\text{xc}}^{\text{LRC(d)}}$. Note that head-only or diagonal LRC kernels reduce the exciton Hamiltonian building time drastically because this removes the double loop over \mathbf{G}, \mathbf{G}' in Eq. (11).

It turns out that the body of $f_{\text{xc}}^{\text{LRC(d)}}$ has a negligible effect on optical spectra of semiconductors such as Si [17]: this is because $\bar{\alpha} \approx 0.2 \ll 4\pi$ in Eq. (16). However, $f_{\text{xc}}^{\text{LRC(h)}}$ and $f_{\text{xc}}^{\text{LRC(d)}}$ can produce very different results for insulators, and one needs to state clearly which version, (h) or (d), of the xc kernel is used.

2. Bootstrap kernels

The original Bootstrap kernel is a parameter-free xc kernel for optical spectra of semiconductors and insulators [19]. The original Bootstrap kernel is defined as

$$f_{\text{xc},\mathbf{G}\mathbf{G}'}^{\text{B}}(\mathbf{q},\omega) = \frac{V_{\mathbf{G}}^{1/2}(\mathbf{q})\epsilon_{\mathbf{G}\mathbf{G}'}^{-1}(\mathbf{q},0)V_{\mathbf{G}'}^{1/2}(\mathbf{q})}{1 - \epsilon_{\text{RPA},00}(\mathbf{q},0)}, \quad (17)$$

where ϵ^{-1} is the self-consistent (i.e., bootstrapped) inverse dielectric function. In matrix form, the bootstrap kernel is given by

$$f_{\text{xc}}^{\text{B}} = \begin{pmatrix} \frac{\beta_{00}}{\mathbf{q}^2} & \frac{\beta_{01}}{|\mathbf{q}||\mathbf{G}_1|} & \frac{\beta_{02}}{|\mathbf{q}||\mathbf{G}_2|} & \cdots \\ \frac{\beta_{10}}{|\mathbf{G}_1||\mathbf{q}|} & \frac{\beta_{11}}{\mathbf{G}_1^2} & \frac{\beta_{12}}{|\mathbf{G}_1||\mathbf{G}_2|} & \cdots \\ \frac{\beta_{21}}{|\mathbf{G}_2||\mathbf{q}|} & \frac{\beta_{21}}{|\mathbf{G}_2||\mathbf{G}_1|} & \frac{\beta_{22}}{\mathbf{G}_2^2} & \cdots \\ \vdots & \vdots & \vdots & \ddots \end{pmatrix}, \quad (18)$$

where

$$\beta_{\mathbf{G}\mathbf{G}'} = \frac{4\pi\epsilon_{\mathbf{G}\mathbf{G}'}^{-1}(\mathbf{q},0)}{1 - \epsilon_{\text{RPA},00}(\mathbf{q},0)}. \quad (19)$$

Neglecting the wings and body of f_{xc}^{B} , which can be viewed as neglecting the LFE, yields a head-only Bootstrap kernel:

$$f_{\text{xc}}^{\text{B(h)}} = \begin{pmatrix} \frac{\beta_{00}}{\mathbf{q}^2} & 0 & 0 & \cdots \\ 0 & 0 & 0 & \cdots \\ 0 & 0 & 0 & \cdots \\ \vdots & \vdots & \vdots & \ddots \end{pmatrix}. \quad (20)$$

Comparing $f_{\text{xc}}^{\text{B(h)}}$ with $f_{\text{xc}}^{\text{LRC(h)}}$, we define the LRC α -parameter for the Bootstrap kernel as

$$\alpha_{\text{B}} = \frac{4\pi\epsilon_{00}^{-1}(0,0)}{\epsilon_{\text{RPA},00}(0,0) - 1}. \quad (21)$$

Whereas $f_{\text{xc}}^{\text{LRC(d)}}$ and $f_{\text{xc}}^{\text{LRC(h)}}$ give quite different results for insulators, we have found that f_{xc}^{B} and $f_{\text{xc}}^{\text{B(h)}}$ make a relatively

small difference (i.e., on the order of $\sim 10\%$) for both semiconductors and insulators (see Table I in Supplemental Material [34]), which is consistent with the findings of Refs. [19] and [20]. In Ref. [21] the same trend was found in the JGM kernel (see below). Therefore, in view of the reduced computational effort, we use the head-only form for all kernels in the following unless stated otherwise. The only exception is when we verify the results of Dyson-equation optical spectra obtained from f_{xc}^{B} using Casida-equation calculations (see Table I in Supplemental Material[34]). We emphasize again that we only consider the $\mathbf{q} \rightarrow 0$ limit here; at finite \mathbf{q} , the matrix character of the Bootstrap kernel appears to play a more significant role [35].

We also consider two simpler variations of the Bootstrap kernel. The first one, referred to as the 0-Bootstrap kernel [36], is the head-only Bootstrap kernel Eq. (20) without the built-in self-consistency (i.e., ‘‘0’’ means no iteration, similar to the G_0W_0 version of the GW approach) for optical spectra of semiconductors and insulators. The LRC α -parameter for the 0-Bootstrap kernel is thus given by

$$\alpha_{0\text{B}} = \frac{4\pi\epsilon_{\text{RPA},00}^{-1}(0,0)}{\epsilon_{\text{RPA},00}(0,0) - 1}. \quad (22)$$

Note that $\alpha_{0\text{B}} > \alpha_{\text{B}}$ by about 10% because $\epsilon_{\text{RPA},00}^{-1}(0,0)$ is greater than $\epsilon_{00}^{-1}(0,0)$ by about 10%.

The second simplified Bootstrap kernel is the RPA-Bootstrap kernel [20], which is a head-only kernel with

$$\alpha_{\text{RPAB}} = \frac{4\pi\epsilon_{\text{RPA},00}^{-1}(0,0)}{1/\epsilon_{\text{RPA},00}^{-1}(0,0) - 1} \quad (23)$$

for exciton binding energies of insulators. Note that $\alpha_{\text{RPAB}} > \alpha_{0\text{B}}$ by about 10% because $1/\epsilon_{\text{RPA},00}^{-1}(0,0) - 1 < \epsilon_{\text{RPA},00}(0,0) - 1$ by about 10%. Note also that without the LFE (i.e., when $\epsilon_{00} = 1/\epsilon_{00}^{-1}$), the 0-Bootstrap and RPA-Bootstrap kernels become identical.

3. Jellium with a gap model

The JGM kernel is a parameter-free kernel for optical spectra of semiconductors and insulators [21]. The JGM kernel is defined as

$$f_{\text{xc}}^{\text{JGM}}(\mathbf{q}; n, E_{\text{g}}) = \frac{4\pi}{\mathbf{q}^2} \left(\frac{B(n) + E_{\text{g}}}{1 + E_{\text{g}}} \right) [e^{k'_{n,E_{\text{g}}}\mathbf{q}^2} - 1] - \frac{4\pi}{k_{\text{F}}^2} \frac{\mathbf{q}^2}{(\mathbf{q}^2 + 1)} \frac{C(n)}{1 + E_{\text{g}}}, \quad (24)$$

with

$$k'_{n,E_{\text{g}}} = k_n + \frac{E_{\text{g}}^2}{4\pi n \mathbf{q}^2} \left(\frac{1 + E_{\text{g}}}{B(n) + E_{\text{g}}} \right). \quad (25)$$

Here, E_{g} is the band gap, n is the electron density, and k_{F} is the Fermi wave vector; k_n , $B(n)$, and $C(n)$ are defined in Ref. [37].

$f_{xc,GG'}^{JGM}(\mathbf{q}; E_g)$ is defined as a full matrix, obtained from the Fourier transform in reciprocal space and the symmetrization in \mathbf{G}, \mathbf{G}' ; however, we here use it in the head-only form. We obtain α_{JGM} values very similar to Ref. [21] (e.g., 0.21 and 0.22, respectively, for GaAs). Whereas other LRC-type kernels depend on dielectric constants, the JGM kernel depends on band gaps.

C. Computational aspects

We used the Abinit code [38], which is based on Troullier-Martins (TM) norm-conserving pseudopotentials, for calculating the Kohn-Sham band structures, including scissors corrections, as well as GW band gaps within the LDA. Experimental lattice parameters were used for all materials. We used the dp code [39] for calculating optical spectra from the imaginary part of the dielectric function. We calculated exciton binding energies from the Casida equation with our own homemade code.

Optical spectra were obtained with a Lorentzian broadening of 0.15 eV for GaAs and 0.2 eV for all other materials, which is a common choice in the excitonic literature. The Lorentzian broadening has a physical meaning, i.e., it simulates the lifetime broadening, so it should not be used as an adjustable parameter to improve the appearance of calculated optical spectra. In principle, the broadening can be calculated from the imaginary parts of GW eigenvalues [40], and there will also be contributions to the broadening from phonons and disorder, but such calculations are beyond the scope of this paper. Note that for a Lorentzian broadening smaller than 0.15 eV, which is an optimal value that makes calculated and experimental E_2 peaks have similar heights, the E_1 peak height in the excitonic region of the RPA and LRC spectra of GaAs is artificially enhanced, and the RPA and LRC E_2 peaks appear higher than the experimental one; thus, such a small broadening should not be used (see the top panel of Fig. 2 for E_1 and E_2 peaks).

We used experimental band gaps, E_g^{exp} , rather than GW band gaps, E_g^{GW} , as fundamental gaps, marking the onsets of the continuous part of the optical spectra. The reason is that there are differences on the order of 1 eV between GW and experimental band gaps in wide-gap insulators. As shown below, these differences are comparable to the exciton binding energies, which are obtained from the difference between fundamental and optical gaps, in the materials under consideration, and can therefore cause an artificial cancellation of the two errors in E_g and E_b when one compares the excitonic peak position in the calculated optical spectrum using E_g^{GW} with the experimental optical spectrum.

In the Dyson equation for optical spectra, we used a $16 \times 16 \times 16$ Monkhorst-Pack \mathbf{k} -point mesh, 4 valence bands, and 20 conduction bands. We found that TDDFT-LRC shows a slower convergence with respect to the number of conduction bands (N_c) than the BSE (e.g., for LiF, $N_c = 6$ is enough for the BSE [2], while $N_c \geq 12$ is needed for both Dyson and Casida equations). An insufficient number of conduction bands causes blueshifts of the excitonic peak (i.e., decreases the exciton binding energy) and reduces its oscillator strength in the LRC spectrum of wide-gap insulators significantly. This slow convergence also occurs for the real part of $\epsilon_M^{\text{LRC}}(\omega = 0)$ (i.e., the LRC dielectric constant).

In the Dyson equation for Bootstrap-type kernel parameters, we used a $20 \times 20 \times 20$ ($20 \times 20 \times 10$) Γ -centered \mathbf{k} -point mesh, 4 (8) valence bands, 20 (20) conduction bands, and 59 (73) \mathbf{G} vectors for GaAs, β -GaN, MgO, LiF, solid Ar, and solid Ne (α -GaN and AlN).

In the Casida equation, we used a $28 \times 28 \times 28$ Γ -centered \mathbf{k} -point mesh, 3 valence bands, 2 conduction bands, and 59 \mathbf{G} vectors for GaAs. The corresponding parameters for the other materials are: $16 \times 16 \times 16$, 3, 6, 59 for β -GaN and MgO; $16 \times 16 \times 8$, 6, 9, 73 for α -GaN and AlN; and $8 \times 8 \times 8$, 3, 24, 59 for LiF, solid Ar, and solid Ne.

To calculate α_{JGM} , we used a $8 \times 8 \times 8$ ($8 \times 8 \times 4$) Γ -centered \mathbf{k} -point mesh and 59 (73) \mathbf{G} vectors for GaAs, β -GaN, MgO, LiF, solid Ar, and solid Ne (α -GaN and AlN).

All computational parameters listed here were chosen after performing systematic convergence tests.

D. Effect of the scissors shift on LRC results

The exact xc kernel can be written in the form $f_{xc} = f_{xc}^{\text{qp}} + f_{xc}^{\text{ex}}$ [5,41], where the ‘‘quasiparticle’’ part, f_{xc}^{qp} , is responsible for correcting the Kohn-Sham gap, and f_{xc}^{ex} is the excitonic part. In the standard TDDFT approach for semiconductors and insulators [3,6,42], the quasiparticle part of f_{xc} is ignored, and any corrections to the Kohn-Sham gap are made directly in the input band structure, usually by means of GW or hybrid functionals; the remaining part of the xc kernel, f_{xc}^{ex} , is then approximated.

A standard and inexpensive method for correcting LDA band structures is by applying the so-called scissors shift [43,44]. There are several ways of applying the scissors shift to Dyson and Casida equations in Eqs. (3), (4), (11), and (16) and LRC-type kernels. The scissors shift can be applied to only the conduction bands (i.e., replacing E_{ck} by $E_{ck} + \Delta$) or to the momentum operator as well (i.e., replacing \hat{p} by $\hat{p}_{\text{renorm}} = \{(E_{ck} + \Delta - E_{vk}) / (E_{ck} - E_{vk})\} \hat{p}$, where \hat{p}_{renorm} is the renormalized momentum operator) [43,45], where Δ is the difference between the experimental (or GW) and DFT band gaps.

Excitonic effects within the LRC approximation are quite sensitive to the particular implementation of the scissors shift. For example, Table I shows α and E_b of GaAs and solid Ne obtained from the RPA-Bootstrap kernel using different types of the scissors shift. We find that the scissors shift affects the LRC results significantly.

In the following, we choose not to apply the scissors shift to E_{ck} and \hat{p} , i.e., we calculate exciton binding energies from the Casida equation using the uncorrected LDA band structure as input. Optical spectra, obtained from the Dyson-equation

TABLE I. LRC kernel parameters α and exciton binding energies E_b (in meV) obtained from the RPA-Bootstrap kernel using different types of the scissors shift.

Scissors shift		GaAs		Ne	
$E_{ck} \rightarrow E_{ck} + \Delta$	$\hat{p} \rightarrow \hat{p}_{\text{renorm}}$	α	E_b	α	E_b
Yes	Yes	0.116	0.601	37.5	6000
Yes	No	0.284	0.246	66.7	7420
No	No	0.073	0.344	30.9	2400

approach, are also calculated based on the uncorrected LDA band structure, and then rigidly shifted to align them with the experimental band gap. We have chosen this approach for several reasons.

First, the scissors shift is not related to excitons. The scissors shift is a matter of choice for the study of excitonic effects in solids. Our aim is to make the simplest choices (e.g., the LDA and the head-only kernel) and to focus on identifying the origin of conflicting results in existing kernels and designing a new kernel. Note that we applied the scissors shift to $E_{c\mathbf{k}}$ and \hat{p} to reproduce the results of existing kernels, which are provided in the Supplemental Material [34].

Second, we were concerned about the unphysically strong influence of the scissors shift on the LRC results. The scissors shift increases ϵ_{00}^{-1} by $\sim 10\%$; this small increase in ϵ_{00}^{-1} affects the LRC results for wide-gap insulators significantly when the LRC-type kernel depends on the dielectric constant (see below). In other words, $f_{xc}^{ex} = f_{xc}^{ex}(f_{xc}^{qp})$, but this is not what f_{xc}^{qp} and f_{xc}^{ex} are meant to be. The big change in the LRC results due to the scissors shift is not associated with excitons.

Third, it allows us to eliminate one source of conflicting results. Some kernels use E_g^{GW} in the scissors shift, compare their optical spectra with experiment, and reproduce or predict the excitonic peak position for wide-gap insulators by interpreting the ~ 1 eV error in E_g^{GW} as E_b [19,25]. In addition, the small difference between E_g^{exp} and E_g^{GW} (or E_g^{GW} obtained from different potential methods) makes a small difference in the scissors-shifted dielectric constant, which can cause a big difference in the LRC results for wide-gap insulators. By not using the scissors shift, we can avoid these unnecessary complications.

Last, by not using the scissors shift we can avoid expensive E_g^{GW} calculations for unknown materials when we need only E_b . When E_g^{GW} is not calculated and the dielectric constant is calculated from density-functional perturbation theory (DFPT) [26,46], which is computationally much cheaper than the sum-over-states (SOS) method Eq. (6) because conduction bands are not needed, large-scale or high-throughput screening exciton calculations become possible.

III. RESULTS AND DISCUSSION

A. Comparison of LRC α -parameters

In the following, we will discuss our results for the excitonic properties of the bulk semiconductors GaAs, α -GaN, and β -GaN, the narrow-gap insulators AlN and MgO, and the wide-gap insulators LiF, solid Ar, and solid Ne. The experimental exciton binding energies are obtained from Refs. [47–54]. We point out again that all results shown below were obtained without using the scissors shift.

Let us begin with an assessment of the LRC α -parameters for various materials. Figure 1 compares α_{LRC} , α_{JGM} , α_B , α_{OB} , and α_{RPAB} with the α -parameter α_{exp} , which, when used in the head-only LRC kernel Eq. (14), reproduces the experimental exciton binding energy for each material under consideration. We see that α varies from ~ 0.1 (α_{RPAB} for GaAs) to ~ 30 (α_{RPAB} for solid Ne). All calculated α -parameters are smaller than the experimentally fitted ones.

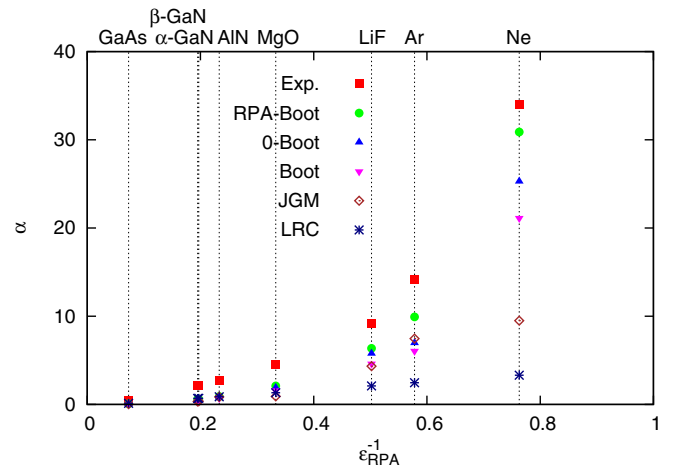


FIG. 1. LRC kernel α -parameters for various materials, compared with the α -parameter fitted to reproduce the experimental exciton binding energy (see text).

B. Sensitivity of optical spectra to changes in α

Next, we examine the effects of the head-only LRC kernel on optical absorption spectra. Figure 2 shows calculated optical spectra of GaAs and solid Ne obtained from the Dyson equation using the LRC kernel with $\alpha = A\alpha_{RPAB}$, where A is a scaling factor, and compares them with experiment [47,52]. We chose GaAs and solid Ne because they are extreme examples of semiconductors with weakly bound Wannier-Mott excitons and insulators with strongly bound Frenkel excitons. In the case of GaAs, the optical spectrum shows two prominent peaks above the band gap; E_1 can be interpreted as a continuum exciton. The bound exciton below the gap is very weak and not visible on the scale of this plot because E_b is much smaller than the line broadening. To see the bound Wannier-Mott exciton of GaAs, high-resolution spectroscopy at low temperatures is needed [55]. On the other hand, for solid Ne the excitonic peak is very prominent and far from the gap, and it is easy to obtain E_b from the spectrum.

In the top panel of Fig. 2, we show calculated optical spectra of GaAs for a range of A between 0.8 and 4.0. We find that the spectra are rather insensitive to the scaling: a 10% change in α has only a very small effect; in other words, α has a big margin for semiconductors. The RPA spectrum of GaAs is already quite similar to experiment, apart from the height of the E_1 -peak. To obtain the experimental height of the E_1 -peak, a scaling factor of $A \approx 4$ (i.e., $\alpha \approx 0.3$) is needed; however, this also increases the peak width, and the valley between the E_1 and the E_2 peak becomes too high.

The bottom panel of Fig. 2 shows the calculated spectra of solid Ne for a much smaller range of A , between 0.8 and 1.1. Here, the spectra are very sensitive to the change in α : a 10% change shifts excitonic peaks by about 1 eV; in other words, α has a small margin for insulators. Clearly, the RPA spectrum of Ne is completely different from experiment, and the LRC kernel reshapes it significantly. Using $A \approx 1.1$ puts the excitonic peak at the right position; however, the peak height and width is now drastically overestimated.

The low sensitivity of LRC results for semiconductors to changes in α explains why there are so many LRC-type

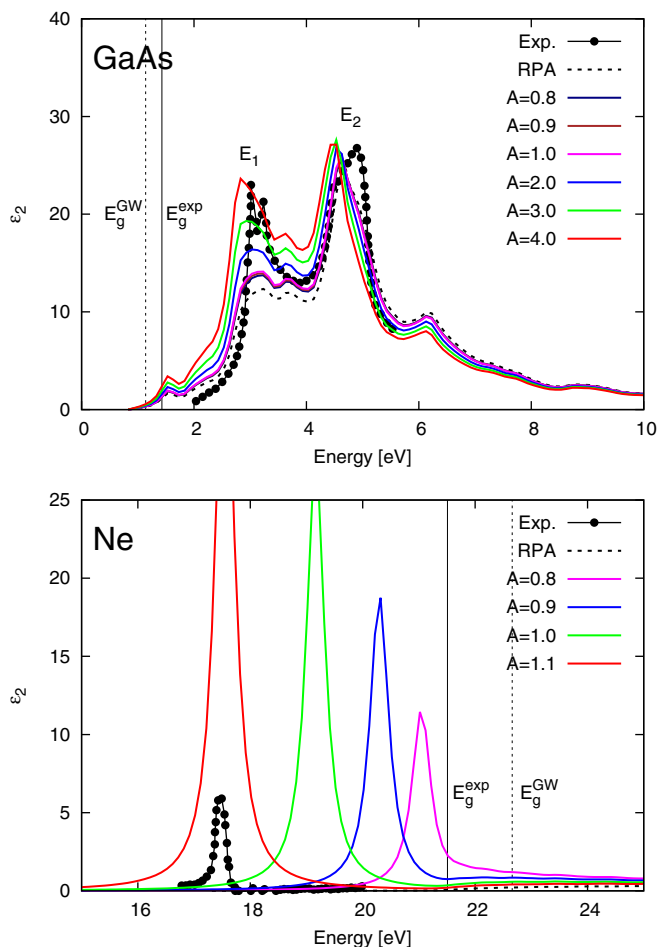


FIG. 2. Experimental and calculated optical absorption spectra of GaAs (top) and solid Ne (bottom). For the LRC kernel, $\alpha = A\alpha_{\text{RPAB}}$ is used, where $\alpha_{\text{RPAB}} = 0.073$ and 30.9 for GaAs and solid Ne, respectively. Note that $A = 0.8$ and 0.9 approximately correspond to Bootstrap and 0-Bootstrap kernels, respectively. The E_1 and E_2 peaks in the spectrum of GaAs are at critical points, where conduction and valence bands are parallel to each other.

kernels. LRC-type kernels only slightly modify RPA spectra of semiconductors, which are already very close to experiment, and α has a big margin for semiconductors. Thus, all LRC-type kernels produce similar and seemingly good optical spectra of semiconductors even when they use different choices and yield very different α values (e.g., $\alpha_{\text{LRC}} \approx 0.2$ and $\alpha_{\text{B}} \approx 0.1$ for Si and GaAs).

The high sensitivity of LRC results for insulators to changes in α is consistent with the finding of Ref. [20]. The idea of the RPA-Bootstrap kernel is to increase E_{b} for wide-gap insulators from ~ 0.1 to ~ 1 eV by increasing α_{B} by $\sim 20\%$ for all materials. However, the $\sim 20\%$ increase in α_{B} does not fix the problem of the Bootstrap kernel of not reproducing an excitonic peak in the optical spectrum of semiconductors, such as Si, because of the low α -sensitivity of LRC results for semiconductors.

We also point out that the LRC results show a similar sensitivity trend to diagonal versus head-only LRC kernels and full versus TDA Casida equations (i.e., insensitive for semiconductors but sensitive for insulators) [33].

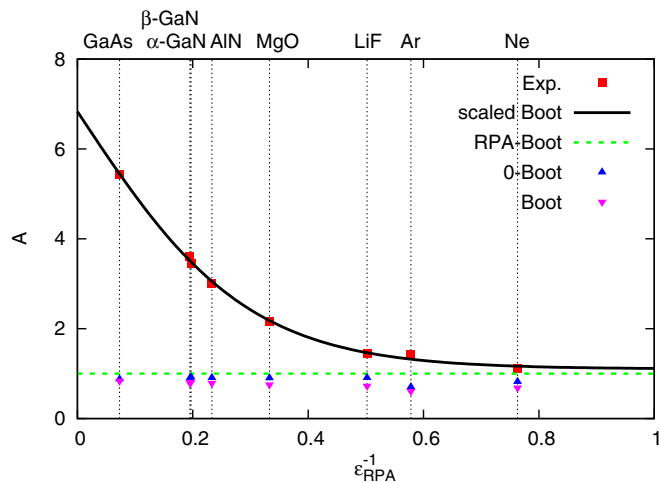


FIG. 3. Scaling factors A_{B} , $A_{0\text{B}}$, and A_{exp} (see text) of Bootstrap-type kernels for various materials.

These two examples already indicate a general limitation of the LRC kernel that applies to *all* materials: it is impossible to obtain the correct position and the correct height and width of an excitonic peak in the LRC spectrum, for *both* semiconductors and insulators. We will provide more evidence for this conclusion and give more examples below. To reproduce a given excitonic feature for both semiconductors and insulators (e.g., the peak height or the peak position), it is clear that a nonuniform scaling factor for Bootstrap-type kernels will be needed: the scaling factor should be close to 1 for insulators but much greater than 1 for semiconductors. Any method that nearly uniformly scales Bootstrap-type kernels for all materials [such as using different dielectric constants (e.g., bootstrapped versus not, scissors-shifted versus not, macroscopic versus microscopic, or RPA versus LDA, all of which are different from each other by $\sim 10\%$) in the numerator and/or the denominator of Eqs. (17), (21), (22), and (23) or using different band structures] is likely to fail to produce satisfactory results across the board.

C. Nonuniformly scaled bootstrap kernel

In Fig. 1 we compared the α values from head-only LRC-type kernels for various materials and found that for wide-gap insulators, α_{RPAB} shows the most similar trend to α_{exp} (e.g., Bootstrap and 0-Bootstrap kernels yield E_{b} of solid Ar that is smaller than that of LiF). We therefore choose it as the basis for constructing a new, scaled Bootstrap xc kernel.

Let us first define $f_{\text{xc}}^{\text{B(h)}} = A_{\text{B}} f_{\text{xc}}^{\text{RPAB}}$ and $f_{\text{xc}}^{\text{0B}} = A_{0\text{B}} f_{\text{xc}}^{\text{RPAB}}$. The values of A_{B} and $A_{0\text{B}}$ are plotted in Fig. 3 as a function of $\epsilon_{\text{RPA}}^{-1}$ for various materials; we find that $A_{\text{B}} \approx 0.8$ and $A_{0\text{B}} \approx 0.9$ for all materials (i.e., Bootstrap-type kernels are nearly uniformly scaled to each other). On the other hand, if we define $f_{\text{xc}}^{\text{exp}} = A_{\text{exp}} f_{\text{xc}}^{\text{RPAB}}$ (i.e., $\alpha_{\text{exp}} = A_{\text{exp}} \alpha_{\text{RPAB}}$) as the head-only LRC xc kernel, which reproduces the experimental exciton binding energy, we can see that A_{exp} varies strongly as a function of material, from ~ 1.1 (solid Ne) to ~ 5 (GaAs). This nonuniform variation is consistent with our observations from the optical spectra of GaAs and solid Ne; see Fig. 2.

The values of A_{exp} show a rather smooth behavior as a function of $\epsilon_{\text{RPA}}^{-1}$, which suggests that a scaled Bootstrap kernel

TABLE II. Fitting parameters for the scaling factor A .

x	a_1	a_2	a_3	a_4	b_1	b_2	b_3	b_4
$\epsilon_{\text{LDA(DFPT)}}^{-1}$	25.9	-0.159	0.161	1.16	6.89	1.11	0.166	1.16
$\epsilon_{\text{RPA(SOS)}}^{-1}$	11.6	-0.00239	0.148	1.10	5.56	1.25	0.155	1.11

can be defined via a fit to the experimental data:

$$f_{xc}^{\text{sB}} = A(x)f_{xc}^{\text{RPAB}} = -A(x)\frac{4\pi x}{(1/x - 1)\mathbf{q}^2}, \quad (26)$$

where $x = \epsilon_{\text{RPA}}^{-1}$ (alternatively, choosing $x = \epsilon_{\text{LDA}}^{-1}$ would have been possible as well). Note that both SOS and DFPT methods yield the same x value [26]. Among many ϵ^{-1} , we used $\epsilon_{\text{RPA(SOS)}}^{-1}$ and $\epsilon_{\text{LDA(DFPT)}}^{-1}$ in this work because they can be easily obtained from the Abinit code. Among the two ϵ^{-1} , we used $\epsilon_{\text{RPA(SOS)}}^{-1}$ to obtain E_b and optical spectra in this work unless stated otherwise.

We found two fitting functions, which describe well the nonuniformity of A_{exp} ,

$$A(x) = \frac{a_1}{e^{(x-a_2)/a_3} + 1} + a_4, \quad (27)$$

$$= b_1 e^{-x^{b_2}/b_3} + b_4. \quad (28)$$

The fitting parameters a_i and b_i , where $i = 1, 2, 3, 4$, are summarized in Table II. Note that these fitting parameters are appropriate for the specific choices made here: experimental lattice constant, TM pseudopotential method, LDA band structure, head-only LRC kernel, LFE, and no scissors shift. If other choices are made, such as all-electron method or scissors shift, one needs to refit the parameters a_i and b_i . This calibration is inevitable due to the high sensitivity of the LRC results for wide-gap insulators. We found that the two fitting functions yield almost the same result for A (and thus α and E_b) except for $\epsilon_\infty \gg 10$ (see Table III). Among the two fitting functions, we chose to use Eq. (28) to obtain E_b and optical spectra.

Figure 4 and Table III show experimental and calculated E_b of various materials. Whereas other kernels underestimate E_b for all materials by ~ 10 times, the scaled Bootstrap kernel yields accurate and consistent E_b . The most significant deviations are for AlN (where all other kernels give zero exciton binding energy) and for solid Ar (where even the BSE underestimates E_b by ~ 0.3 eV [56]).

 TABLE III. Experimental and calculated exciton binding energies E_b (in meV).

		GaAs	α -GaN	β -GaN	AlN	MgO	LiF	Ar	Ne	
Exp.		3.27	20.4	26.0	48.0	80.0	1600	1900	4080	
scaled Boot	$\epsilon_{\text{LDA(DFPT)}}^{-1}$	Eq. (27)	3.30	23.1	21.4	97.4	90.1	1790	1230	5220
scaled Boot	$\epsilon_{\text{LDA(DFPT)}}^{-1}$	Eq. (28)	3.30	23.0	21.4	97.4	92.3	1790	1230	5190
scaled Boot	$\epsilon_{\text{RPA(SOS)}}^{-1}$	Eq. (27)	3.24	22.2	22.1	90.4	97.2	1710	1220	5410
scaled Boot	$\epsilon_{\text{RPA(SOS)}}^{-1}$	Eq. (28)	3.24	22.1	22.0	90.6	102	1720	1210	5350
RPA-Boot			0.344	1.06	1.01	0.00	2.12	94.7	96.0	2400
0-Boot			0.293	0.919	0.829	0.00	1.72	43.2	13.7	612
Boot			0.278	0.735	0.649	0.00	1.20	14.8	9.14	101
JGM			0.141	0.438	0.279	0.00	0.397	12.1	17.1	5.96
LRC			0.670	1.33	1.32	0.00	0.855	1.89	1.54	1.06

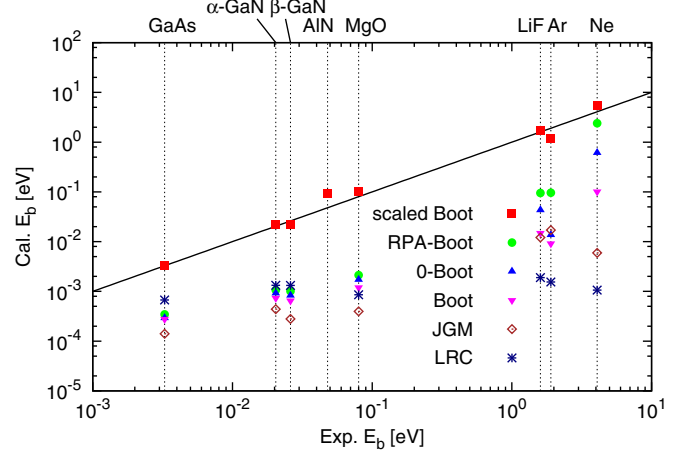


FIG. 4. Comparison of experimental and calculated exciton binding energies E_b for various materials, using LRC-type xc kernels. The solid straight line indicates perfect agreement between theory and experiment.

Figure 5 shows experimental and calculated optical spectra of GaAs, MgO, LiF, and solid Ne. We included LiF because it is one of two extreme examples of wide-gap insulators. We also included MgO because the LRC spectrum of MgO is very different from experiment at all α values, so it is impossible to determine an optimal α value for MgO by varying α (i.e., no α exists that reproduces the correct excitonic peak height or position) [17]. Here, we report the LRC spectrum of MgO when $\alpha \approx \alpha_{\text{exp}}$. Bootstrap-type kernels with similar α values produce very similar optical spectra of GaAs (a semiconductor) and MgO (a narrow-gap insulator), but very different ones of LiF and solid Ne (wide-gap insulators). As discussed earlier, this is due to the different sensitivity of LRC spectra to semiconductors and insulators.

Our scaled Bootstrap kernel, which is designed to reproduce E_b^{exp} , yields excitonic peaks with overestimated (i.e., higher and wider) oscillator strengths in optical spectra of GaAs and MgO, while other Bootstrap-type kernels, which underestimate E_b by ~ 10 times, barely produce excitonic peaks. This indicates that the LRC kernel cannot produce correct exciton binding energies and optical spectra at the same time for *all* materials (i.e., for semiconductors *and* insulators). Our finding is consistent with the LRC spectrum of ZnO, in which the

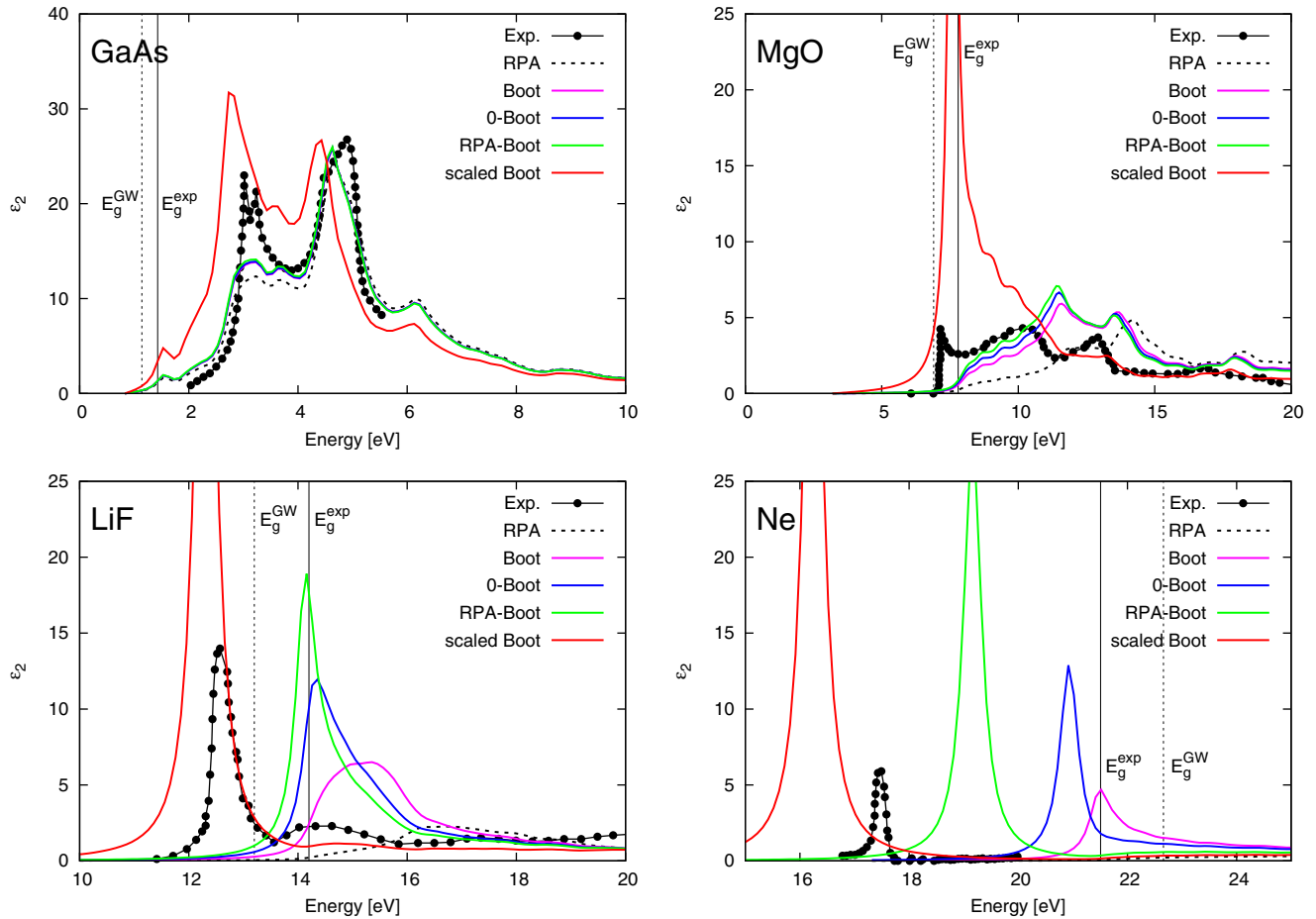


FIG. 5. Experimental and calculated optical absorption spectra of GaAs, MgO, LiF, and solid Ne. The origins of the different results for LiF between Refs. [19] and [20] (see also Ref. [7]) and this work are explained in the Supplemental Material [34].

calculated excitonic peak is much higher and wider than the experimental one [57].

We emphasize that our kernel is empirical, but *universal* in that it works for all materials and all choices. In contrast, the RPA-Bootstrap kernel, one of parameter-free kernels, works only for wide-gap insulators under special conditions such as experimental lattice parameters, the head-only kernel, and the scissors shift. In principle, a parameter-free LRC-type kernel cannot be universal for all choices due to the high sensitivity of LRC results for wide-gap insulators; thus, a tradeoff between parameter-free and universal is unavoidable.

Our scaling approach is not just another Bootstrap-type kernel or a correction to the RPA-Bootstrap kernel: it is a method to predict E_b of unknown materials using the experimental E_b of a few known materials as input. The RPA-Bootstrap kernel is merely used as a fitting function, which was chosen to demonstrate the problems of popular Bootstrap-type kernels [19,20,25] and to suggest a simple way to fix them. One has the full freedom to use any other LRC-type fitting functions for our method.

IV. CONCLUSIONS

In this paper, we have carried out a systematic numerical assessment of the family of static long-range-corrected (LRC) xc kernels for solids. The main challenge faced by TDDFT for

the optical spectral properties of semiconductors and insulators is to reproduce the excitonic peaks at the right position and with the correct strength. We have used two methods: the Dyson-equation approach, which yields optical spectra, and the Casida-equation approach, which allows a precise determination of exciton binding energies. The two methods are equivalent, i.e., they give, in principle, the same excitonic peak positions, but in their practical implementations they are very different: from the Dyson equation approach, and the resulting macroscopic dielectric function, one cannot extract the binding energies of weakly bound excitons. Hence, the Casida approach is a very useful method, complementing the standard Dyson approach.

We have studied a group of materials, ranging from small-gap semiconductors to large-gap insulators, with exciton binding energies between a few meV and several eV. For these materials, we have tested the empirical LRC kernel, several flavors of the Bootstrap kernel, and the jellium-with-a-gap model. Most of these methods produce decent looking optical spectra for semiconductors, but the exciton binding energies are consistently underestimated. We proposed a new xc kernel, obtained via a material-dependent scaling of the RPA-Bootstrap kernel. The scaled Bootstrap kernel is designed to produce accurate exciton binding energies for all materials under study, at very low computational cost. However, there is a price to pay: it turns out that it is impossible to obtain

accurate exciton binding energies and good optical spectra at the same time for all materials using any LRC method—if the exciton peak is at the right place, the oscillator strength (i.e., the peak height and width) tends to be exaggerated for both semiconductors and insulators.

In general, assessing the performance of xc kernels for excitonic properties is a delicate task, because there are many choices involved. Here, we chose to use LDA band structures obtained with a pseudopotential code, we included local-field effects, and we implemented the xc kernels in their head-only forms. These choices will affect the numerical results: whereas the spectra of semiconductors are relatively insensitive to the strength α of the head of the LRC kernel, the spectra of insulators are very sensitive. Hence, it is crucial that all choices made are clearly identified, in order to facilitate comparison between results obtained by different research groups.

The main outcome of our work is that we have developed a method that can produce accurate exciton binding energies at a low computational cost. In practice, the parameters for the scaling function should be refitted for each particular implementation, using a small test set of small- and large-gap materials. It should then be possible to obtain accurate exciton binding energies for other, more complicated materials. Such calculations are currently in progress.

The ultimate goal is to develop TDDFT approaches that yield both accurate exciton binding energies and spectral shapes. As we have seen, the LRC method is too restricted to achieve both. TDDFT is in principle exact; however, going

beyond the LRC approach is very challenging: we will need to better understand the role of the wings and body of the xc kernel. To see why this is so, notice that purely short-range xc kernels can produce excitons if the xc kernel is used in full matrix form, and if the kernels are sufficiently strong [an extreme example is the so-called contact exciton [18], but even the adiabatic LDA (ALDA) can produce excitons if it is scaled up by several orders of magnitude]. Thus, in view of the results presented in this paper, one concludes that a new form of the xc kernel is necessary, in which the short-range and long-range behaviors may be equally important: both must be taken into account and built into the full matrix form of the xc kernel. In addition, the frequency dependence of the xc kernel may have to be taken into account, in particular if the goal is to produce an excitonic Rydberg series. Alternatives beyond pure TDDFT, such as hybrid functionals, are therefore very promising. Such methods are currently under development.

ACKNOWLEDGMENTS

This work was supported by NSF Grant No. DMR-1408904. The computation for this work was performed on the high performance computing infrastructure provided by Research Computing Support Services at the University of Missouri-Columbia. We thank Lucia Reining and Sangeeta Sharma for discussions and for providing valuable comments on the manuscript.

-
- [1] A. Miyata, A. Mitioglu, P. Plochocka, O. Portugall, J. T.-W. Wang, S. D. Stranks, H. J. Snaith, and R. J. Nicholas, *Nat. Phys.* **11**, 582 (2015).
 - [2] M. Rohlfing and S. G. Louie, *Phys. Rev. Lett.* **81**, 2312 (1998).
 - [3] G. Onida, L. Reining, and A. Rubio, *Rev. Mod. Phys.* **74**, 601 (2002).
 - [4] R. M. Martin, L. Reining, and D. M. Ceperley, *Interacting Electrons: Theory and Computational Approaches* (Cambridge University Press, Cambridge, 2016).
 - [5] C. A. Ullrich, *Time-dependent Density-functional Theory: Concepts and Applications* (Oxford University Press, Oxford, 2012).
 - [6] C. A. Ullrich and Z.-H. Yang, in *Density-Functional Methods for Excited States*, Topics in Current Chemistry, Vol. 368, edited by N. Ferré, M. Filatov, and M. Huix-Rotllant (Springer, Berlin, 2015), p. 185.
 - [7] N. T. Maitra, *J. Chem. Phys.* **144**, 220901 (2016).
 - [8] L. Reining, V. Olevano, A. Rubio, and G. Onida, *Phys. Rev. Lett.* **88**, 066404 (2002).
 - [9] F. Sottile, V. Olevano, and L. Reining, *Phys. Rev. Lett.* **91**, 056402 (2003).
 - [10] G. Adragna, R. Del Sole, and A. Marini, *Phys. Rev. B* **68**, 165108 (2003).
 - [11] A. Marini, R. Del Sole, and A. Rubio, *Phys. Rev. Lett.* **91**, 256402 (2003).
 - [12] P. J. Stephens, F. J. Devlin, C. F. Chabalowski, and M. J. Frisch, *J. Phys. Chem.* **98**, 11623 (1994).
 - [13] L. Bernasconi, S. Tomić, M. Ferrero, M. Rérat, R. Orlando, R. Dovesi, and N. M. Harrison, *Phys. Rev. B* **83**, 195325 (2011).
 - [14] S. Tomić, L. Bernasconi, B. G. Searle, and N. M. Harrison, *J. Phys. Chem. C* **118**, 14478 (2014).
 - [15] S. Refaely-Abramson, M. Jain, S. Sharifzadeh, J. B. Neaton, and L. Kronik, *Phys. Rev. B* **92**, 081204 (2015).
 - [16] Z.-H. Yang, F. Sottile, and C. A. Ullrich, *Phys. Rev. B* **92**, 035202 (2015).
 - [17] S. Botti, F. Sottile, N. Vast, V. Olevano, L. Reining, H.-C. Weissker, A. Rubio, G. Onida, R. Del Sole, and R. W. Godby, *Phys. Rev. B* **69**, 155112 (2004).
 - [18] S. Botti, A. Schindlmayr, R. Del Sole, and L. Reining, *Rep. Prog. Phys.* **70**, 357 (2007).
 - [19] S. Sharma, J. K. Dewhurst, A. Sanna, and E. K. U. Gross, *Phys. Rev. Lett.* **107**, 186401 (2011).
 - [20] S. Rigamonti, S. Botti, V. Veniard, C. Draxl, L. Reining, and F. Sottile, *Phys. Rev. Lett.* **114**, 146402 (2015).
 - [21] P. E. Trevisanutto, A. Terentjevs, L. A. Constantin, V. Olevano, and F. D. Sala, *Phys. Rev. B* **87**, 205143 (2013).
 - [22] S. Sharma, J. K. Dewhurst, A. Sanna, and E. K. U. Gross, *Phys. Rev. Lett.* **117**, 159701 (2016).
 - [23] S. Rigamonti, S. Botti, V. Veniard, C. Draxl, L. Reining, and F. Sottile, *Phys. Rev. Lett.* **117**, 159702 (2016).
 - [24] S. Botti, A. Fourreau, F. Nguyen, Y.-O. Renault, F. Sottile, and L. Reining, *Phys. Rev. B* **72**, 125203 (2005).
 - [25] J. A. Berger, *Phys. Rev. Lett.* **115**, 137402 (2015).
 - [26] M. Gajdoš, K. Hummer, G. Kresse, J. Furthmüller, and F. Bechstedt, *Phys. Rev. B* **73**, 045112 (2006).
 - [27] S. Baroni and R. Resta, *Phys. Rev. B* **33**, 7017 (1986).

- [28] M. E. Casida, in *Recent Advances in Density Functional Methods*, Recent Advances in Computational Chemistry, Vol. 1, edited by D. E. Chong (World Scientific, Singapore, 1995), pp. 155–192.
- [29] P. Ghosez, X. Gonze, and R. W. Godby, *Phys. Rev. B* **56**, 12811 (1997).
- [30] Y.-H. Kim and A. Görling, *Phys. Rev. B* **66**, 035114 (2002).
- [31] Z.-H. Yang, Y. Li, and C. A. Ullrich, *J. Chem. Phys.* **137**, 014513 (2012).
- [32] Z.-H. Yang and C. A. Ullrich, *Phys. Rev. B* **87**, 195204 (2013).
- [33] Y.-M. Byun and C. A. Ullrich, *Computation* **5**, 9 (2017).
- [34] See Supplemental Material at <http://link.aps.org/supplemental/10.1103/PhysRevB.95.205136> for technical details of the bootstrapping algorithm, effects of the scissors shift on exciton binding energies, and a comparison with results from the literature.
- [35] S. Sharma, J. K. Dewhurst, A. Sanna, A. Rubio, and E. K. U. Gross, *New J. Phys.* **14**, 053052 (2012).
- [36] S. Sharma (private communication).
- [37] L. A. Constantin and J. M. Pitarke, *Phys. Rev. B* **75**, 245127 (2007).
- [38] X. Gonze, B. Amadon, P.-M. Anglade, J.-M. Beuken, F. Bottin, P. Boulanger, F. Bruneval, D. Caliste, R. Caracas, M. Côté, T. Deutsch, L. Genovese, P. Ghosez, M. Giantomassi, S. Goedecker, D. Hamann, P. Hermet, F. Jollet, G. Jomard, S. Leroux, M. Mancini, S. Mazevet, M. Oliveira, G. Onida, Y. Pouillon, T. Rangel, G.-M. Rignanese, D. Sangalli, R. Shaltaf, M. Torrent, M. Verstraete, G. Zerah, and J. Zwanziger, *Comput. Phys. Commun.* **180**, 2582 (2009).
- [39] V. Olevano, L. Reining, and F. Sottile, <http://www.dp-code.org/>.
- [40] M. Cazzaniga, H.-C. Weissker, S. Huotari, T. Pykkänen, P. Salvestrini, G. Monaco, G. Onida, and L. Reining, *Phys. Rev. B* **84**, 075109 (2011).
- [41] R. Stubner, I. V. Tokatly, and O. Pankratov, *Phys. Rev. B* **70**, 245119 (2004).
- [42] S. Sharma, J. K. Dewhurst, and E. K. U. Gross, in *First Principles Approaches to Spectroscopic Properties of Complex Materials*, Topics in Current Chemistry, Vol. 347, edited by C. D. Valentin, S. Botti, and M. Cococcioni (Springer, Berlin, 2014), p. 235.
- [43] Z. H. Levine and D. C. Allan, *Phys. Rev. Lett.* **63**, 1719 (1989).
- [44] X. Gonze and C. Lee, *Phys. Rev. B* **55**, 10355 (1997).
- [45] R. Del Sole and R. Girlanda, *Phys. Rev. B* **48**, 11789 (1993).
- [46] S. Baroni, S. de Gironcoli, A. Dal Corso, and P. Giannozzi, *Rev. Mod. Phys.* **73**, 515 (2001).
- [47] M. Parenteau, C. Carlone, and S. M. Khanna, *J. Appl. Phys.* **71**, 3747 (1992).
- [48] D. J. As, F. Schmilgus, C. Wang, B. Schöttker, D. Schikora, and K. Lischka, *Appl. Phys. Lett.* **70**, 1311 (1997).
- [49] J. F. Muth, J. H. Lee, I. K. Shmagin, R. M. Kolbas, H. C. Casey, B. P. Keller, U. K. Mishra, and S. P. DenBaars, *Appl. Phys. Lett.* **71**, 2572 (1997).
- [50] R. Haensel, G. Keitel, E. E. Koch, M. Skibowski, and P. Schreiber, *Phys. Rev. Lett.* **23**, 1160 (1969).
- [51] D. M. Roessler and W. C. Walker, *J. Opt. Soc. Am.* **57**, 835 (1967).
- [52] V. Saile and E. E. Koch, *Phys. Rev. B* **20**, 784 (1979).
- [53] R. A. R. Leute, M. Feneberg, R. Sauer, K. Thonke, S. B. Thapa, F. Scholz, Y. Taniyasu, and M. Kasu, *Appl. Phys. Lett.* **95**, 031903 (2009).
- [54] D. M. Roessler and W. C. Walker, *Phys. Rev.* **159**, 733 (1967).
- [55] R. G. Ulbrich, *Adv. Solid State Phys.* **25**, 299 (1985).
- [56] F. Sottile, M. Marsili, V. Olevano, and L. Reining, *Phys. Rev. B* **76**, 161103 (2007).
- [57] P. Gori, M. Rakel, C. Cobet, W. Richter, N. Esser, A. Hoffmann, R. Del Sole, A. Cricenti, and O. Pulci, *Phys. Rev. B* **81**, 125207 (2010).